Journal of Materials Science: Materials in Electronics (2019) 30:8055–8063
https://doi.org/10.1007/s10854-019-01127-0

Enhanced photocatalytic performance of $ZnFe_2O_4$/BiOI hybrid for the degradation of methyl orange

Menghan Zhang[1] · Xin Xie[1] · Yushan Si[1] · Jie Gao[1] · Hongnan Du[1] · Shuxin Pei[1] · Xinyu Zhang[1] · Qishe Yan[1]

Received: 8 December 2018 / Accepted: 12 March 2019 / Published online: 16 March 2019

Abstract
The $ZnFe_2O_4$/BiOI hybrid photocatalysts were fabricated by the solvothermal method. The crystalline phase, morphologies composition and optical absorption property of the samples with different $ZnFe_2O_4$ contents were analyzed utilizing XRD, SEM, PL and UV–vis diffuse reflection spectrum, respectively. The photocatalytic activities of the as-prepared photocatalysts were evaluated by degrading methyl orange (MO) under visible light irradiation. Compared with pure BiOI and pure $ZnFe_2O_4$ catalyst, $ZnFe_2O_4$/BiOI hybrid photocatalysts could observably enhance photocatalytic activity and the 5% $ZnFe_2O_4$/BiOI composite performed the optimal degradation efficiency (81.2%) in 100 min. The kinetic studies indicated that the photodegradation followed the first-order kinetic reaction model. Free radical trapping tests illustrated that $^{\cdot}O_2^-$ and h^+ play the key roles in catalytic reaction. In consequence, the $ZnFe_2O_4$/BiOI composite can be widely used to treat organic pollutant in wastewater.

1 Introduction

With the development of society, the rapid growing of urbanization and industrialization, the shortage of clean water resource stands out in the world and water pollution becomes a serious problem [1–3]. Among various contaminants in the water, the organic dyes have become significant because the synthetic organic dyes are widely used in various industries including textile, cosmetic, paper, leather, etc [4–7]. As we known, synthetic dyes is discovered at nineteenth century [8, 9] and it is difficult to removal due to its large production and difficult degradation [5, 10]. There are numerous hazardous chemicals in the dye wastewater, and their existence has already threatened the better quality of people and animals' living standard [8]. Hence, it is important to remove the hazardous chemicals from water [8, 11]. In order to solve this problem, lots of methods have been experimented by researchers in the last year [8]. With the development of science and technology, the photocatalysis is coming into horizon.

As an efficient and safe environmental purification technology, photocatalytic technology has been widely applied to the degradation of hazardous chemicals [12]. Well, the searching of high-efficiency photocatalytic materials is the key to apply photocatalytic technology in the treatment of hazardous chemicals [13]. Photocatalytic materials refer to a kind of semiconductor materials that can induce photo-redox reaction under illumination. As a semiconductor photocatalyst which has been studied for decades, titanium dioxide (TiO_2) is non-toxic, stable, low-cost and readily available [14, 15], but it only shows photocatalytic activity under ultraviolet light because of the wide band gap, and the photocatalytic activity is greatly restricted owing to the recombination of electron–hole pairs [16]. Therefore, the researchers are committed to finding a better photocatalytic material for pollutants degradation, and the bismuth-based catalysts possessing the special layered structure and internal electric field have attracted the attention of researchers due to its good visible light response properties [17]. Among bismuth-based catalysts, bismuth oxyhalides (BiOX, X = F, Cl, Br, I) ternary oxide semiconductors have been intensively investigated owing to its remarkable photocatalytic activities, and BiOI displays outstanding photocatalytic activity because of its narrower band gap [18–20]. Nevertheless, it is still of importance to further improve its photocatalytic efficiency in order to be suitable for practical applications [21, 22]. So it is significant to improve separation efficiency of the

✉ Qishe Yan
qisheyanzzu@163.com

[1] Institution of Chemistry and Molecular Engineering, Zhengzhou University, No. 100, Science Avenue, Zhengzhou, Henan, China

photo-generated electron–hole pair of BiOI photocatalyst. In order to achieve the above purpose, researchers improve the photocatalytic activity of BiOI by various strategies, such as metal doping, non-metallic doping and construction heterojunction, etc [23, 24]. Due to the unique physical and chemical properties, the spinel-structured ferrite nanoparticles catch the attention of researchers, and as the important type of the spinel-structured ferrite, the zinc ferrite ($ZnFe_2O_4$) with a narrow band gap engages more attention due to the excellent visible-light response, good photochemical stability, low toxicity and superior magnetic separable property [25–30]. Therefore, the $ZnFe_2O_4$ can be selected to dope with the BiOI to improve the photo reactivity.

In this work, the BiOI with different morphologies and $ZnFe_2O_4$ catalysts were prepared by a simple solvothermal and hydrothermal methods, respectively. The BiOI with the best morphology was selected to prepare $ZnFe_2O_4$/BiOI hybrid photocatalysts by the solvothermal method. Methyl orange (MO) was chosen as targeted pollutant to evaluate the photocatalytic performance and the results showed that the $ZnFe_2O_4$ amount displayed important influence on the photocatalyst activity.

2 Experimental

2.1 Chemical materials

All chemicals were of analytical grade (A.R.) and used without further purification. Sodium nitrate pentahydrate ($Bi(NO_3)_3{\cdot}5H_2O$), ferric chloride ($FeCl_3$) and sodium hydroxide (NaOH) were all purchased from Tianjin Kermel Chem. Reagent Co. Ltd. Ethylene glycol ($(CH_2OH)_2$) and absolute ethyl alcohol (CH_3CH_2OH) were obtained from Tianjin Dern Chem. Reagent Co. Ltd. Potassium iodide (KI) was bought from Tianjin Bodi chemical Industry Co. Ltd. Zinc nitrate hexahydrate ($Zn(NO_3)_2{\cdot}6H_2O$) was purchased from Shanghai Macklin Biochemical Co. Ltd. Ammonium hydroxide was acquired from Yantai Shuangshuang Chemical Industry Co. Ltd. The deionized water was used for all synthesis and treatment.

2.2 Synthesis of $ZnFe_2O_4$/BiOI composites

2.2.1 Synthesis of BiOI

BiOI was synthesized by solvothermal method at a certain temperature and reaction time. Different structural morphologies can be controlled by changing the pH and solvent of the solution. Briefly, 0.970 g $Bi(NO_3)_3{\cdot}5H_2O$ and 0.332 g KI were dissolved into 38 mL absolute ethanol and distilled water, respectively. The KI solution was added dropwise into the $Bi(NO_3)_3$ solution under magnetic stirring. After that, the mixed solution was adjusted to pH 9 by ammonium hydroxide ($NH_3{\cdot}H_2O$) under vigorous stirring. And then, the mixed solution was transferred to a 100 mL autoclave and reacted for 24 h at 140 °C. Afterwards, the precipitate was removed and washed several times with deionized water and absolute ethanol, and dried at 80 °C. The resulting sample was recorded as BI-a. Besides, the pH value of the mixture solution was adjusted to 11 with other conditions unchanged, the acquired sample was denoted as BI-b. Similarly, changing the solvent of $Bi(NO_3)_3$ solution from absolute ethanol to ethylene glycol and the pH of the mixture solution from 9 to 11 while the others remain the same, the prepared sample was recorded as BI-c.

2.2.2 Synthesis of $ZnFe_2O_4$

$ZnFe_2O_4$ photocatalyst was synthesized by hydrothermal method. According to this method, 1 mmol $Zn(NO_3)_2{\cdot}6H_2O$ and 2 mmol $FeCl_3{\cdot}6H_2O$ were dissolved in 30 mL deionized water. Then, 5 mL NaOH (3 mol/L) was added dropwise into above mixture solution at room temperature and stirred for 10 min. After that, the mixture solution was injected into 50 mL reaction kettle under 180 °C for 15 h. The precipitate was washed several times with deionized water and ethanol, respectively, and dried at 120 °C for 8 h.

2.2.3 Synthesis of $ZnFe_2O_4$/BiOI composites

A series of $ZnFe_2O_4$/BiOI photocatalyst composites were synthesized by solvothermal method. A certain amount of the as-prepared $ZnFe_2O_4$ and 1.94 g $Bi(NO_3)_3{\cdot}5H_2O$ were added into ethylene glycol, 0.67 g KI was also dissolved in ethylene glycol with continual stirring. Then the KI solution was added into the $Bi(NO_3)_3{\cdot}5H_2O$ solution drop-by-drop, and the pH value of the mixed solution was adjusted to 11 and making the above mixture solution ultrasonic smash for 10 min to get the stable solution. Then, the mixture solution was injected into 100 mL reaction kettle under 140 °C for 24 h. The precipitate was washed with deionized water and ethanol, respectively, and dried at 80 °C. The prepared samples are $ZnFe_2O_4$/BiOI hybrid photocatalysts. The catalysts were designed as 3%, 5%, 7% and 10% $ZnFe_2O_4$/BiOI photocatalytic composite materials.

2.3 Characterization

Scanning electron microscopy (SEM) images were observed on a Hitachi TM-1000 microscope. The X-ray diffraction (XRD) analysis were carried out with an X-ray diffractometer (D/MAX-r A, Rigaku, Japan) equipped with a Cu KαX-ray source ($\lambda = 1.5405$ Å) and operated at a voltage of 50 kV and a current of 50 mA, in the 2θ range from 5° to 90° at a scanning step of 0.02°. UV–Vis diffuse reflection

spectra (UV–Vis DRS) were performed by using a UV–Vis spectrophotometer (Caly 5000, Agilent, USA) and $BaSO_4$ was used as the reflectance. The photoluminescence (PL) spectroscopy was measured at the excitation wavelength of 420 nm on F-7000 Fluorescence Spectrophotometer. Photoelectrochemical measurements were carried out on an electrochemicalanalyzer (CHI660E electrochemical station, CHI Instruments Inc.) with a standard three-electrode system.

2.4 Photocatalytic activity measurement

The photocatalytic activity of the as-prepared samples was evaluated by the degradation of MO in aqueous solutions (0.02 g/L) under simulated solar light irradiation. A 300 W Xe lamp was served as a simulated light source to trigger the photocatalytic reaction. In each experiment, 0.02 g photocatalyst was added to 50 mL MO solution and dispersed by ultrasonic for 3 min. After that, the suspension was continuously stirred by a dynamoelectric stirrer under the irradiation and 2 mL solution was sampled at the given time intervals (10 min) during the irradiation. Filtered the catalyst and the filtrate was analyzed by UV–vis spectrometer (UV-2450 Shimadzu, Japan).

The photocatalytic activity can be reflected on this equation:

$$D = \frac{C_{0-}C_t}{C_0} \times 100\%$$

where D is the degradation rate, C_0 is the initial concentration of MO solution, and C_t is the concentration of MO solution after t min radiation.

In the degradation, the value variation of the chemical oxygen demand (COD) indicated the degradation degree of MO in the solutions. The value of COD was measured by potassium dichromate titration and determined by a closed microwave digestion instrument.

3 Results and discussion

3.1 Characterization analysis

The crystalline phase and crystallinity of the as-prepared samples were investigated via X-ray diffraction (XRD). Figure 1 shows the XRD patterns of BI-a, BI-b, BI-c, $ZnFe_2O_4$, and $ZnFe_2O_4$/BiOI photocatalytic materials. As can be seen from the XRD patterns of BiOI catalysts, the diffraction peaks located at about 28°, 45° and 55° became sharper as the pH increased, the intensity of diffraction peaks located at 10°, 28°, 32°, 45° and 55° decreased and the impurity peaks disappeared when the ethylene glycol displaced anhydrous ethanol, suggesting that the BI-c

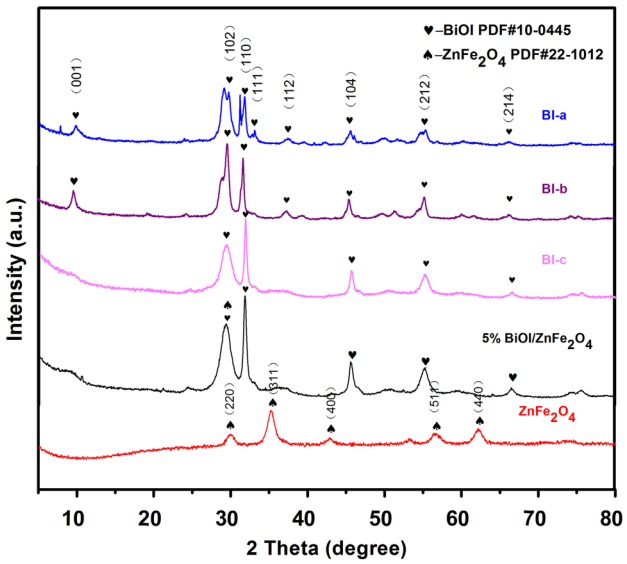

Fig. 1 XRD patterns of the as-prepared samples (BI-a: pH 9; BI-b: pH 11; BI-c: pH 11/$C_2H_6O_2$; $ZnFe_2O_4$ and 5% $ZnFe_2O_4$/BiOI composite)

was purer. The diffraction peaks of $ZnFe_2O_4$/BiOI complex could be indexed to BI-c and no impurity peaks were observed, which implied a high purity of the composite. Additionally, there was no diffraction peak of $ZnFe_2O_4$ catalyst appearing in the XRD pattern of 5% $ZnFe_2O_4$/BiOI composite and the diffraction peaks of $ZnFe_2O_4$/BiOI composite became sharper with the introduction of $ZnFe_2O_4$ particles, which indicated that the addition of $ZnFe_2O_4$ particles just influenced the diffraction intensity of BiOI, rather than the structure of the peak.

The scanning electron microscopy (SEM) was used to detect the morphologies and microstructure of the as-prepared samples. Figure 2 presents the SEM images of BI-a (Fig. 2A1, A2), BI-b (Fig. 2B1, B2), BI-c (Fig. 2C1, C2) and 5% $ZnFe_2O_4$/BiOI photocatalyst (Fig. 2D1, D2). It is obvious that the basic morphologies of BiOI were all the petal-like spherical structures assembled by nano-flakes. The morphology evolution of BiOI microsphere can be speculated, that is, to form nano layers first, and then formed nano layers assemble into flowerlike orbicular structures by themselves. What's more, the BiOI that getting the more beautiful flowerlike orbicular structure when the pH was 11 and the reaction solvent was ethylene glycol had the largest diameter. As can be seen from Fig. 2d, the morphology of BiOI microspheres was changed and the average particle size became smaller after combining with $ZnFe_2O_4$ particles. The surface structure of $ZnFe_2O_4$/BiOI compound was assembled by a large number of sheet structures where large quantities of $ZnFe_2O_4$ particles attached, meaning that $ZnFe_2O_4$ particles were successfully composited with BiOI particles. This structure enlarged the surface area of the hybrid and

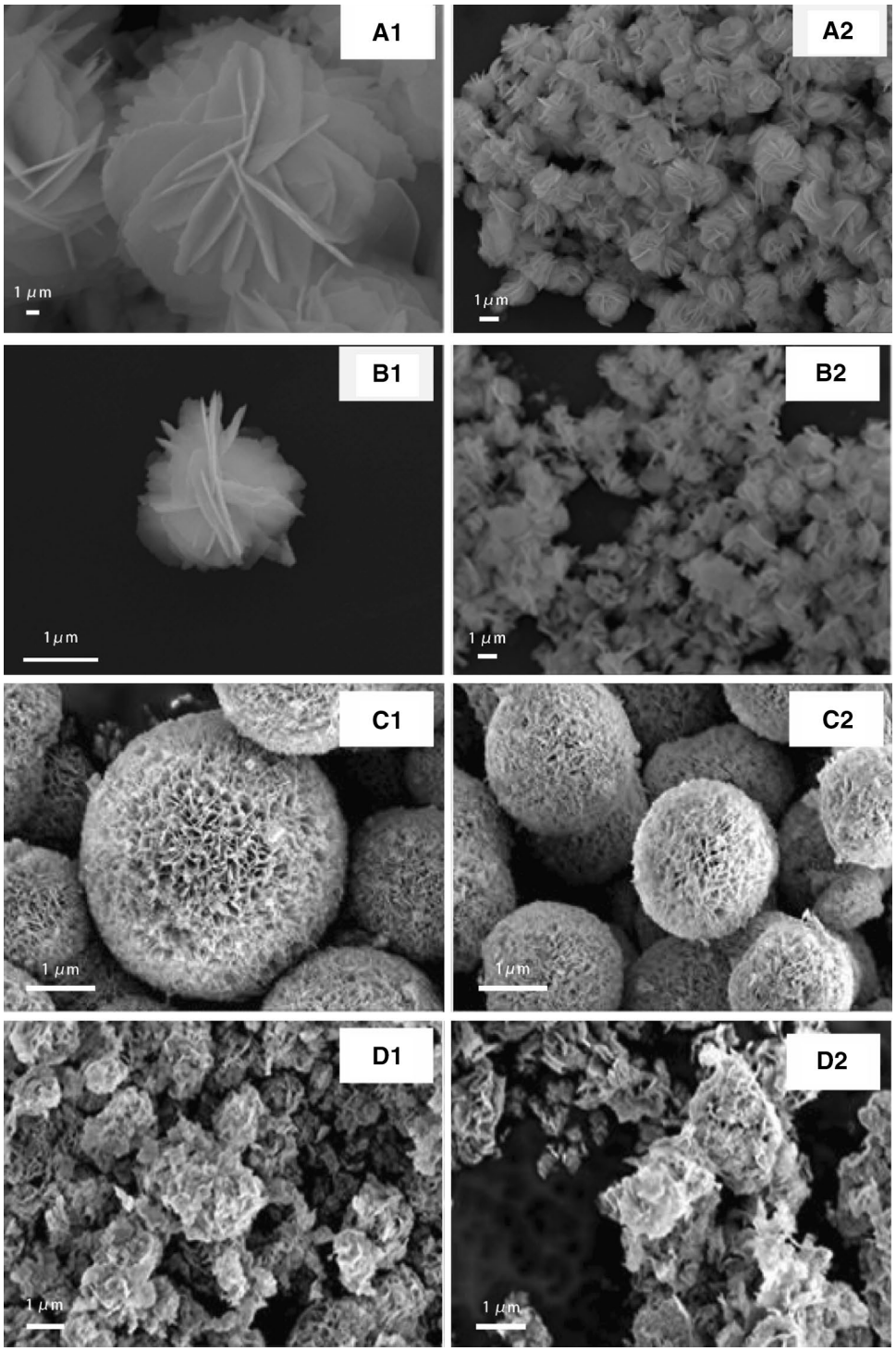

Fig. 2 SEM images of all samples. **A1, A2: BI**-a (pH 9); **B1, B2**: BI-b (pH 11); **C1, C2**: BI-c (pH 11/$C_2H_6O_2$); **D1, D2**: 5% $ZnFe_2O_4$/BiOI composite

increased the reaction site of photocatalytic reaction, what is beneficial to enhance photocatalytic activity.

The UV–vis diffuse reflectance spectra (DRS) of the as-synthesized samples were displayed in Fig. 3. It can be noticed that a wide absorption from UV to visible light for all samples. The absorption edges of BI-c, 3% $ZnFe_2O_4$/BiOI, 5% $ZnFe_2O_4$/BiOI, 7% $ZnFe_2O_4$/BiOI and 10% $ZnFe_2O_4$/BiOI were at about 640 nm, 650 nm, 662 nm, 663 nm, 685 nm, respectively. Result indicates that the absorption edges of the composites had a red shift with the introduction of $ZnFe_2O_4$ particles, demonstrating the $ZnFe_2O_4$/BiOI complex exhibited better absorption intensity than BiOI catalyst, which might be benefited to the formation of the photo-generated electron–hole pairs under the visible light irradiation

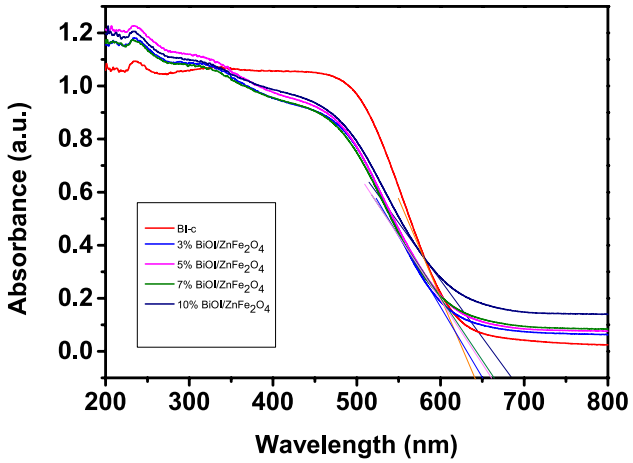

Fig. 3 UV–vis diffuse adsorption spectra of BI-c and series of $ZnFe_2O_4$/BiOI complex

and further to promote the photocatalytic performance. And their band gap energy was calculated by this equation:

$$Eg = 1240/\lambda$$

The λ is the maximum absorption wavelength of photon. The calculated band gap energy of BiOI, 3% $ZnFe_2O_4$/BiOI, 5% $ZnFe_2O_4$/BiOI, 7% $ZnFe_2O_4$/BiOI and 10% $ZnFe_2O_4$/BiOI was 1.94 eV, 1.91 eV, 1.87 eV, 1.87 eV, 1.81 eV, respectively.

In order to research the effect of degradation on the light absorption property of the 5% $ZnFe_2O_4$/BiOI complex, the UV–vis diffuse reflectance spectra (DRS) of the 5% $ZnFe_2O_4$/BiOI photocatalyst before and after MO degradation was shown in Fig. 4. Obviously, the light absorption efficiency of the 5% $ZnFe_2O_4$/BiOI complex before and after MO degradation changed slightly, indicating that the degradation of methyl orange had little effect on the light absorption performance of the compound.

The recombination of the photo-induced electrons and holes would decrease the quantum yield, which affect largely the activity of photocatalytic reaction. The recombination of the electron hole pairs can release energy in the form of fluorescence emissions, which can be captured and showed in photoluminescence spectra. Figure 5 presents the PL spectra of the $ZnFe_2O_4$, BiOI and 5% $ZnFe_2O_4$/BiOI complex. It is shown that the 5% $ZnFe_2O_4$/BiOI complex shows weaker emission peaks compared with $ZnFe_2O_4$ and BiOI. This means that the electron–hole recombination rate of 5% $ZnFe_2O_4$/BiOI complex is decreased, suggesting that the combination of the $ZnFe_2O_4$ and BiOI can improve photocatalytic activity.

The charge separation can be evaluated by transient photocurrent density vs. time curves and the transient photocurrent response of $ZnFe_2O_4$, BiOI and 5% $ZnFe_2O_4$/BiOI compound was shown in Fig. 6 [31, 32]. It is evident that the 5% $ZnFe_2O_4$/BiOI compound has the strongest photocurrent response to all of the samples, illustrating that the composite has more separation efficiency of photo-generated electron–hole pairs, which coincident with the PL results. The enhanced photocurrent may be due to the doping of $ZnFe_2O_4$ and BiOI, the result shows the doping can enhance the separation of photo-generated electron–hole pairs and prolong the photo-generated charge.

To further study the possible photocatalytic enhance mechanism, the Mott-Schottky plots for $ZnFe_2O_4$ and BiOI samples was shown in Fig. 7. The x-intercept of the linear tangent is a flat band potential (E_{FB}) of about −0.62 V and −0.7 V versus an Ag/AgCl electrode for the BiOI and $ZnFe_2O_4$ samples, respectively. Since the E_{FB} is considered approximately as the conduction band (CB) edge, the E_{CB} of the BiOI and $ZnFe_2O_4$ was estimated to be −0.62 V and

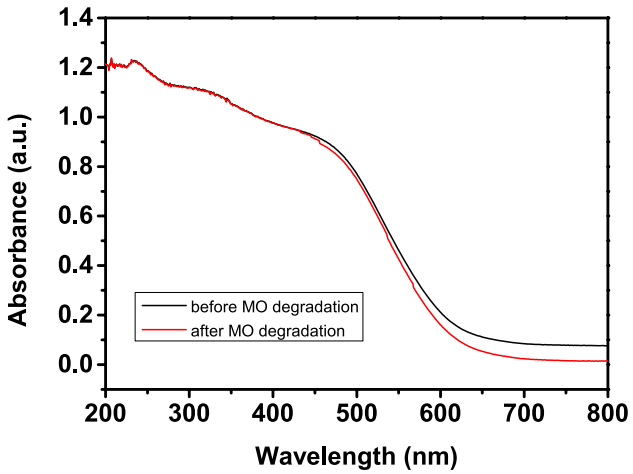

Fig. 4 UV–vis diffuse adsorption spectra of 5% $ZnFe_2O_4$/BiOI complex before and after MO degradation

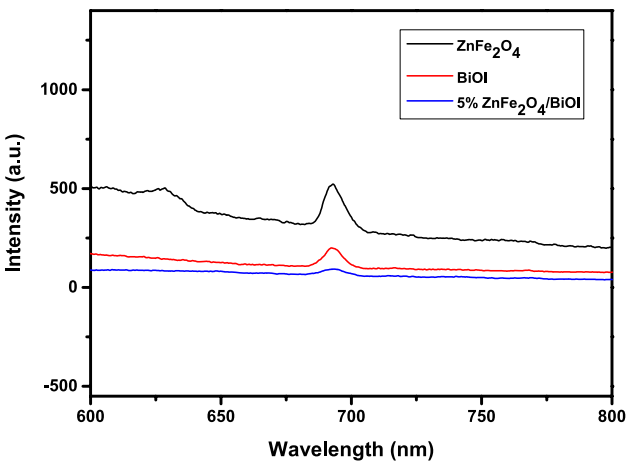

Fig. 5 PL spectra of $ZnFe_2O_4$, BiOI and 5% $ZnFe_2O_4$/BiOI complex

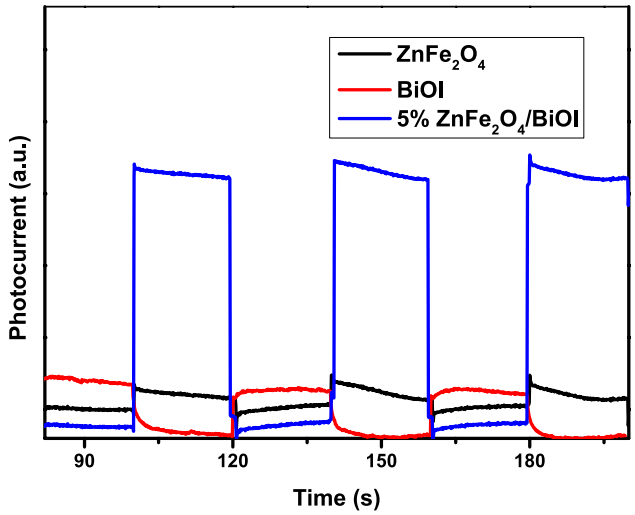

Fig. 6 Photocurrent of $ZnFe_2O_4$, BiOI and 5% $ZnFe_2O_4$/BiOI compound

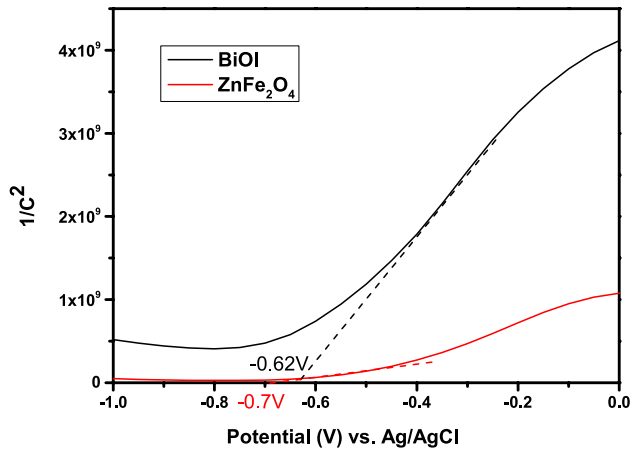

Fig. 7 Mott-Schottky plots of $ZnFe_2O_4$ and BiOI samples

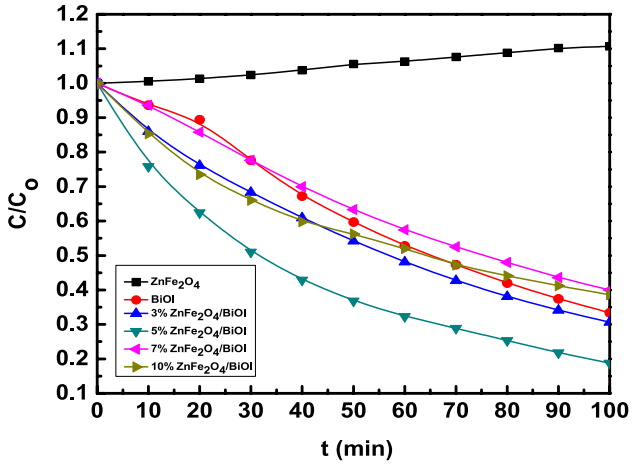

Fig. 8 Photocatalytic degradation of MO with as-prepared catalysts under visible light irradiation

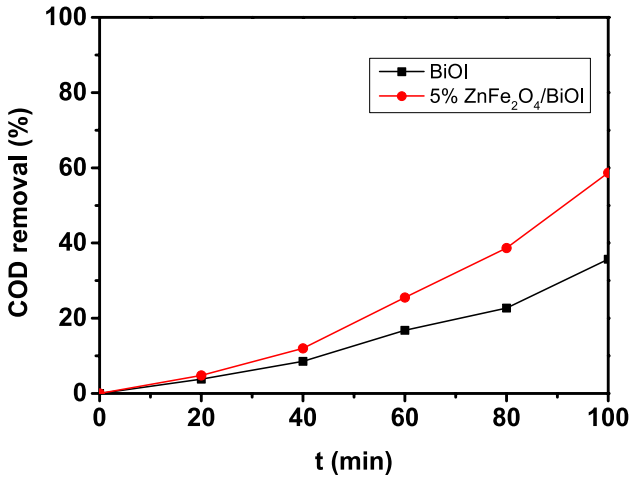

Fig. 9 COD removal of the MO solution with the BiOI and 5% $ZnFe_2O_4$/BiOI compound

− 0.7 V, respectively [33, 34]. The energy positions of the valence band edge (E_{VB}) can be calculated according to the following equation:

$$E_{CB} = E_{VB} - E_g$$

where E_g is the band gap of the semiconductor. The E_{VB} of the BiOI and $ZnFe_2O_4$ was estimated to be 1.28 V and 1.2 V, respectively.

3.2 Photocatalytic properties

The photocatalytic activity of all catalysts was evaluated by the degradation of methyl orange (MO) solution under the simulated solar light irradiation. Figure 8 shows the degradation efficiencies of MO by using the as-prepared samples under illumination. It can be seen that $ZnFe_2O_4$ was bare of photocatalytic activity on degrading MO, even the concentration of MO was increased slightly in the process of degradation. After degrading for 100 min under visible light irradiation, the degradation ratios of 3%, 5%, 7%, and 10% $ZnFe_2O_4$/BiOI composites were 69.4%, 81.2%, 60.0%, 61.4%, respectively. Conspicuously, the 5% $ZnFe_2O_4$/BiOI exhibits the best photocatalytic degradation efficiency.

The COD was frequently used as important indicator to express the relative content of organic matter in contamination solution. Figure 9 represents the COD removal of the methyl orange (MO) solution with the BiOI catalyst and 5% $ZnFe_2O_4$/BiOI compound. It shows that both of the COD removal efficiency enhanced with the increased irradiation time, manifesting that the organic matter in MO solution was degraded. Compared with the 35.68% COD removal by pure BiOI after irradiation time of 100 min, 58.69% of

COD removal efficiency with 5% $ZnFe_2O_4$/BiOI compound indicated that the 5% $ZnFe_2O_4$/BiOI complex was more efficient, suggesting its potential applicability in wastewater treatment.

3.3 Kinetic studies

The relation between ln (C_t/C_0) and t for MO degradation by all samples is shown in Fig. 10. It could be detected that the degradation of MO by the above photocatalysts followed the first-order kinetic reaction model. According to the Langmuir–Hinshelwood equation: ln $(C_t/C_0) = -kt$, where k is rate constant, t is irradiation time, the rate constants (k) of MO degradation using the as-samples could be calculated, as shown in Table 1. It can be seen from Fig. 10 and Table 1, when the $ZnFe_2O_4$ doping contents of $ZnFe_2O_4$/BiOI composites are 3% and 5%, the doping of $ZnFe_2O_4$ can enhance the degradation activity compared with pure BiOI. Nevertheless, the doping of $ZnFe_2O_4$ may reduce the degradation activity when the $ZnFe_2O_4$ doping contents are 7% and 10%. Compared with the k value of 3% (0.0117), 7% (0.00941), 10% (0.0091) $ZnFe_2O_4$/BiOI compounds, the k value of 5% $ZnFe_2O_4$/BiOI (0.01588) was the highest, indicating that the as-prepared $ZnFe_2O_4$/BiOI composite had the best catalytic activity when the loaded $ZnFe_2O_4$ was 5%. It can be concluded that the appropriate doping amount of $ZnFe_2O_4$ can contribute to the separation of electron–hole pairs, thereby improving the photocatalytic degradation efficiency, and the migration of carriers in hindered when the amount is too large, resulting in a decrease in photocatalytic performance.

3.4 Mechanism of photocatalytic activity

To investigate the main active species for the degradation of MO and further understand the reaction mechanism, different kinds of scavengers (ammonium oxalate as scavenger for the h^+, p-benzoquinone (BQ) as scavenger for $\cdot O_2^-$, isopropanol as scavenger for $\cdot OH$) were added into the reaction solutions, respectively. As shown in Fig. 11, the concentration of MO solution increased slightly after the addition of ammonium oxalate into the catalytic degradation process, which indicated that the primary position of the h^+ in the catalytic process. Meanwhile, the photocatalytic efficiency of 5% $ZnFe_2O_4$/BiOI compound was significantly inhibited with the addition of p-benzoquinone, manifesting the $\cdot O_2^-$ was also the main active species in the degradation process. What's more, after the addition of isopropanol into the reaction system, the photodegration efficiency of the 5% $ZnFe_2O_4$/BiOI composite was decreased without significantly compared with the reaction system of no scavengers. According to the results mentioned above, it can be concluded that the $\cdot O_2^-$ and h^+ were both the main active

Table 1 First-order kinetic parameters of MO degradation with as-prepared samples

Sample	Equation	k/min^{-1}	R^2
$ZnFe_2O_4$	$-\ln(C/C_0) = -0.0011\,t + 0.00514$	0.0011	0.991
BiOI	$-\ln(C/C_0) = 0.0115\,t - 0.05868$	0.0115	0.993
3%$ZnFe_2O_4$/BiOI	$-\ln(C/C_0) = 0.0117\,t + 0.02591$	0.0117	0.999
5%$ZnFe_2O_4$/BiOI	$-\ln(C/C_0) = 0.01588\,t + 0.13405$	0.01588	0.983
7%$ZnFe_2O_4$/BiOI	$-\ln(C/C_0) = 0.00941\,t - 0.01918$	0.00941	0.998
10%$ZnFe_2O_4$/BiOI	$-\ln(C/C_0) = 0.0091\,t + 0.0935$	0.0091	0.975

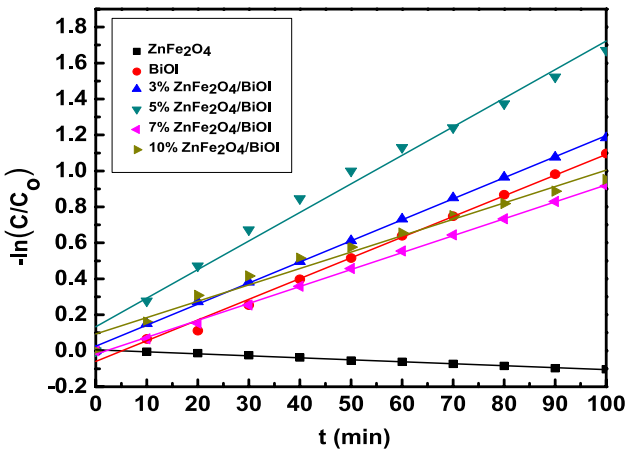

Fig. 10 The first-order reaction kinetics for MO degradation with all samples

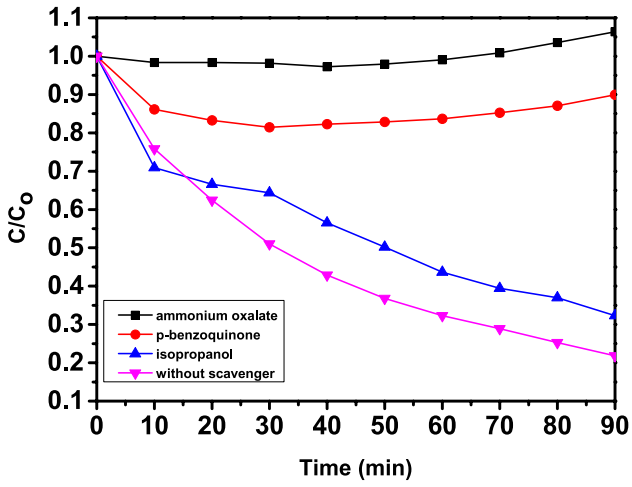

Fig. 11 Effect of different scavengers on the degreadation of MO in presence of 5% $ZnFe_2O_4$/BiOI compound

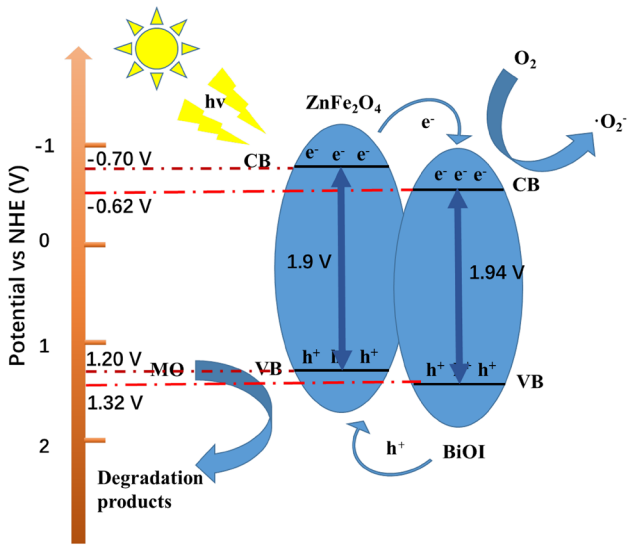

Fig. 12 The photocatalytic mechanism of $ZnFe_2O_4$/BiOI compound

species in the photocatalytic process of 5% $ZnFe_2O_4$/BiOI composite catalyst.

The possible photocatalytic reaction mechanism of $ZnFe_2O_4$/BiOI complex is simply displayed in Fig. 12. Under the visible light irradiation, electrons of $ZnFe_2O_4$ are excited from valance band (VB) to the conduction band (CB) while holes are generated in the VB. These photo-generated electrons can transfer to the CB of BiOI, so it can inhibit the recombination of photo-generated electron pairs. The photo-generated electrons with strong reducibility can be obtained by dissolved oxygen and to form superoxide radical to degrade MO, the holes with strong oxidation can degrade the MO directly. So the possible mechanism is as follow:

$$ZnFe_2O_4 + hv \rightarrow e^-_{CB}\left(ZnFe_2O_4\right) + h^+_{VB}(ZnFe_2O_4)$$

$$e^-_{CB}(BiOI) + O_2 \rightarrow \cdot O_2^-$$

$$\cdot O_2^- + MO \rightarrow \text{Degradation products}$$

$$h^+_{VB}(ZnFe_2O_4) + MO \rightarrow \text{Degradation products}$$

4 Conclusions

In conclusion, series of $ZnFe_2O_4$/BiOI composites and BiOI catalysts were prepared by solvothermal method. The morphologies of BiOI catalysts were slightly different with the different preparation conditions. When the BiOI particles doped with $ZnFe_2O_4$ particles, the microsphere of BiOI was changed and its average particle size became smaller. The degradation of methyl orange (MO) indicated that the introduction of $ZnFe_2O_4$ particles distinctly enhanced the photocatalytic activity of BiOI, and 5% $ZnFe_2O_4$/BiOI composite showed the highest photocatalytic activity (81.2%), which coincident with the results of PL and photocurrent. According to the kinetic studies, it can be detected that the degradation of MO by the $ZnFe_2O_4$/BiOI composites followed the first-order kinetic reaction model and only the appropriate doping amount of $ZnFe_2O_4$ could contribute to the separation of electron–hole pairs, thereby improving the photocatalytic degradation efficiency. Trapping experiments proved that the O_2^- and h^+ play the key role in photocatalytic process. Consequently, as a high performance photocatalyst, $ZnFe_2O_4$/BiOI composites can play a role in organic dyes degradation in wastewater.

Acknowledgements The authors are thankful to the institute of environmental sciences, Zhengzhou University.

References

1. Q. Zhu, N. Liu, N. Zhang, Y.Y. Song, M.S. Stanislaus, C.Y. Zhao, Y.H. Yang, J. Environ. Chem. Eng. **6**(2), 2724 (2018)
2. W. Zhang, H.L. Tay, S.S. Lim, Y.S. Wang, Z.Y. Zhong, R. Xu, Appl. Catal. B Environ. **95**(1–2), 93 (2010)
3. Y.N. Chen, G.Q. Zhu, M. Hojamberdiev, J.Z. Gao, R.L. Zhu, C.H. Wang, X.M. Wei, P. Liu, J. Hazard. Mater. **344**, 42 (2018)
4. P. Kharazi, R. Rahimi, M. Rabbani, Mater. Res. Bull. **103**, 133 (2018)
5. K. He, G.Q. Chen, G.M. Zeng, A.W. Chen, Z.Z. Huang, J.B. Shi, T.T. Huang, M. Peng, L. Hu, Appl. Catal. B Environ. **228**, 19 (2018)
6. M. Nasrollahzadeh, M. Atarod, S.M. Sajadi, Appl. Surf. Sci. **364**, 636 (2016)
7. M. Mahendiran, J.J. Mathen, M. Racik, J. Madhavan, M.V.A. Raj, J. Phys. Chem. Solids **126**, 322 (2019)
8. V. Katheresan, J. Kansedo, S.Y. Lau, J. Environ. Chem. Eng. **6**(4), 4676 (2018)
9. S. Natarajan, H.C. Bajaj, R.J. Tayade, J. Environ. Sci China. **65**, 201 (2018)
10. X. Liu, Y.M. Cheng, X.F. Li, J.F. Dong, Appl. Surf. Sci. **439**, 784 (2018)
11. D. Ayodhya, G. Veerabhadram, Mater. Today Energy. **9**, 83 (2018)
12. M. Yan, Y.Q. Hua, F.F. Zhu, W. Gu, J.H. Jiang, H.Q. Shen, W.D. Shi, Appl. Catal. B Environ. **202**, 518 (2017)
13. Q.S. Yan, X. Xie, C.P. Lin, Y.L. Zhao, S.B. Wang, Y.G. Liu, J. Mater. Sci. Mater. Electron. **28**(22), 16696 (2017)
14. Z.P. Xing, J.Q. Zhang, J.Y. Cui, J.W. Yin, T.Y. Zhao, J.Y. Kuang, Z.Y. Xiu, N. Wan, W. Zhou, Appl. Catal. B Environ. **225**, 452 (2018)
15. S.E. Arasi, M.V.A. Raj, J. Madhavan, J. Mater. Sci. Mater. Electron. **29**, 3170 (2017)
16. T.T. Yang, J.M. Peng, Y. Zheng, X. He, Y.D. Hou, L. Wu, X.Z. Fu, Appl. Catal. B Environ. **221**, 223 (2018)
17. H.C. Lan, G. Zhang, H.W. Zhang, H.J. Liu, R.P. Liu, J.H. Qu, Catal. Commun. **98**, 9 (2017)
18. M.M. Xu, Y.L. Zhao, Q.S. Yan, Water. sci. Technol. **72**(12), 2122 (2015)
19. S.W. Gao, C.S. Guo, S. Hou, L. Wan, Q. Wang, J.P. Lv, Y. Zhang, J.F. Gao, W. Meng, J. Xu, J. Hazard. Mater. **331**, 1 (2017)
20. L.Y. Zhang, Q.S. Yan, Y.Y. Wang, R.Q. Zhang, Synth. React. Inorg. M **45**, 1245 (2015)
21. H. Liu, W.R. Cao, Y. Su, Y. Wang, X.H. Wang, Appl. Catal. B Environ. **111–112**, 271 (2012)

22. X.W. Li, C.G. Niu, D.W. Huang, X.Y. Wang, X.G. Zhang, G.M. Zeng, Q.Y. Niu, Appl. Surf. Sci. **286**, 40 (2013)
23. Y.Z. Hong, C.S. Li, Y.D. Meng, C.Y. Huang, W.D. Shi, Mater. Sci. Eng. B. **224**, 69 (2017)
24. X.C. Meng, Z.S. Zhang, J. Colloid. Interface Sci. **485**, 296 (2017)
25. L.Q. Jing, Y.G. Xu, C.C. Qin, J. Liu, S.Q. Huang, M.Q. He, H. Xu, H.M. Li, Mater. Res. Bull. **95**, 607 (2017)
26. S.K. Wu, X.P. Shen, G.X. Zhu, H. Zhou, Z.Y. Ji, K.M. Chen, A.H. Yuan, Appl. Catal. B Environ. **184**, 328 (2016)
27. L. Chen, W. Ma, J.D. Dai, J. Zhao, C.X. Li, Y.S. Yan, J. Photochem. Photobiol. A. **328**, 24 (2016)
28. C.L. Wang, X. Tan, J.T. Yan, B. Chai, J.F. Li, S.Z. Chen, Appl. Surf. Sci. **396**, 780 (2017)
29. R.C. Sripriya, V.A.F. Samson, S. Anand, J. Madhavan, M.V.A. Raj, J. Mater. Sci. Mater. Electron. **29**, 14084 (2018)
30. Y. Huang, D.D. Zhu, Q. Zhang, Y.F. Zhang, J.J. Cao, Z.X. Shen, W.K. Ho, S.C. Lee, Appl. Catal. B-Environ. **234**, 70 (2018)
31. Y. Huang, Y.X. Gao, Q. Zhang, Y.F. Zhang, J.J. Cao, W.K. Ho, S.C. Lee, J. Hazard. Mater. **354**, 54 (2018)
32. Y.F. Jia, S.P. Li, J.Z. Gao, G.Q. Zhu, F.C. Zhang, X.J. Shi, Y. Huang, C.L. Liu, Appl. Catal. B-Environ. **240**, 241 (2019)
33. G.Q. Zhu, M. Hojamberdiev, S.L. Zhang, S.T.U. Din, W. Yang, Appl. Surf. Sci. **467**, 968 (2019)
34. Q.Z. Wang, T.J. Niu, L. Wang, C.X. Yan, J.W. Huang, J.J. He, H. She, B.T. Su, Y.P. Bi, Chem. Eng. J. **337**, 506 (2018)